

Nuclear Equation of State and the Structure of Neutron Stars

Yeunhwan LIM*

Cyclotron Institute, Texas A&M University, College Station, TX 77843, U.S.A.

Taehyun KIM

Department of Physics, Kyungpook National University, Daegu 41566, Korea

Yongseok OH†

Department of Physics, Kyungpook National University, Daegu 41566, Korea and
 Asia Pacific Center for Theoretical Physics, Pohang 37673, Korea

(Received 6 November 2016 : revised 12 December 2016 : accepted 12 December 2016)

Starting from the binding energies of finite or isolated nuclei, to investigate ways to study inhomogeneous nuclear matter, *i.e.*, nuclei with a free gas of neutrons, we review and discuss a general method to solve the nuclear equation of state for neutron stars by finding the solution for uniform nuclear matter. We also discuss a way to develop the nuclear equation of state in the presence of hyperons. The mass-radius relations of neutron stars are compared with the results of X-ray burst analyses to probe the validities of various models for the nuclear equation of state in neutron star physics.

PACS numbers: 21.30.-x, 21.65.Ef, 26.60.-c

Keywords: Neutron star, Nuclear equation of state, Nuclear properties, Nuclear matter

I. INTRODUCTION

Neutron star is one of the most interesting objects in nuclear astrophysics for it gives a test ground for dense nuclear matter and, besides, it is one of the final stages of stellar evolution. The existence of neutron stars was first expected by W. Baade and F. Zwicky [1] two years after the discovery of the neutron in 1932 by J. Chadwick¹. After more than 30 years of its hiding, it was discovered by A. Hewish and J. Bell in 1967 as a form of radio pulsating object, a pulsar, because of its strong magnetic field and rapid spin. (See, for example, Ref. 3.) The typical radius of neutron stars is around 10 km and the mass goes up to $2.0 M_{\odot}$, with M_{\odot} being the solar mass.

*E-mail: yylim@tamu.edu

†E-mail: yohphy@knu.ac.kr

¹ However, it is also argued that L. Landau suggested the presence of dense matter object in the universe during the discussion with N. Bohr and L. Rosendfeld in 1931 even before the discovery of the neutron. See Ref. 2 for details on this story.

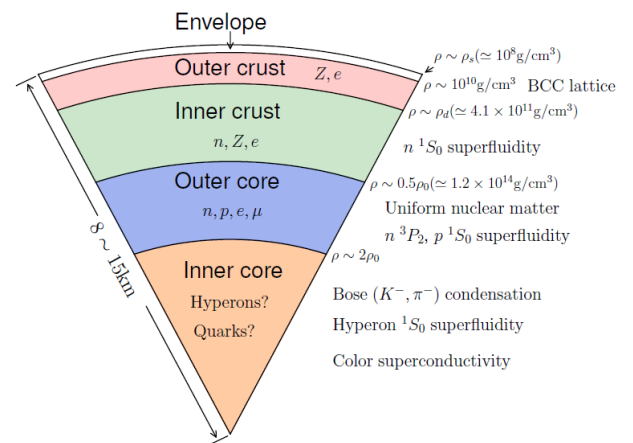


Fig. 1. (Color online) Standard schematic cross sectional picture of a neutron star.

As its name indicates, a neutron star is a highly neutron-rich object. The amount of proton in neutron stars is estimated to be only up to 10% although the fraction depends on the specific nuclear model. Fig. 1 shows the standard picture of the cross sectional struc-



ture of a neutron star. From the outside, there exists envelope on top of the neutron star surface. The envelope is composed of hydrogen or helium depending on the chemical evolution of neutron stars or accreting material from the companion star. Inside the envelope, there is the outer crust where the ionized nuclei have the lattice structure. The ionized nuclei become neutron-rich to minimize the total energy of the nuclear system and neutrons drip out of nuclei. Thus heavy nuclei exist with a free gas of neutrons and they make the inner crust of a neutron star. As the baryon number density increases, heavy nuclei are dissolved to make uniform nuclear matter. The transition density from inhomogeneous nuclear matter to uniform nuclear matter is around $0.5n_0$, where n_0 is the normal nuclear density, $n_0 = 0.16 \text{ fm}^{-3}$. In the outer core of neutron stars, neutrons, protons, electrons, and muons coexist to maintain chemical equilibrium. In the inner core, as baryon number density increases, the distance between nucleons becomes comparable with its size, and then new degrees of freedom come out. As a result, hyperons or quark matter might exist in the core of neutron stars. However, it is still unknown what kinds of particles exist or what kinds of exotic condensations might happen. In other words, there still are many puzzles to be explored to understand the structure of neutron stars, which should be closely related to our understanding of nuclear matter under various conditions.

Recent discoveries of neutron stars with a mass of $2.0 M_\odot$ [4, 5] require construction of new equation of states (EOS) as the existence of such heavy neutron stars rules out soft EOS. Thus these observations require the modification of the current models for EOS and/or nuclear force models. Together with $2.0 M_\odot$ neutron stars, the analyses of X -ray burst data [6,7] also provide a clue of how to modify the nuclear EOS. Namely, the accreting materials from the companion star on the surface of a neutron star are burned out and emit X -rays if the amount of material exceeds the critical mass for hydrogen burning on the surface of the neutron star. The X -ray patterns then specify the allowed region of neutron star radius for a given value of mass.

The central area of neutron stars is estimated to have a density at the order of a few times the nuclear saturation density and it is highly neutron-rich. Such high neutron-rich matter has not been accessible in the laboratory so

far. However, the recent construction of rare isotope accelerators will enable us to explore neutron-rich nuclei. In the present article, we discuss a simple but effective numerical method to compute nuclear EOS. The EOS, of course, should explain the allowed mass-radius region for neutron stars. For this purpose, we work with several nuclear models and confirm the validity of EOS in the mass-radius relations of neutron stars.

This paper is organized as follows. In Sec. II, we introduce the general liquid drop model (LDM) and see the validity of using LDM to calculate binding energies of finite nuclei. In Sec. III, we discuss how to implement LDM to make neutron star crust equation of state. Then, in Sec. IV, the particle components in the core of neutron star are investigated and a new degree of freedom, *i.e.*, strangeness, is studied. To find a new parameter set for the relativistic mean field model, we use the recent calculation of pure neutron matter properties. The obtained mass-radius relation of neutron stars is presented in Sec. V. Finally, we summarize nuclear EOS for dense matter in Sec. VI.

II. NUCLEAR BINDING ENERGY

The binding energy of a nucleus can be obtained using LDM with relatively high accuracy. In LDM, the total binding energy consists of bulk, surface, Coulomb, pairing, and shell energy terms. In the algebraic form, the total binding energy for a nucleus with proton number Z and neutron number N , so that $A = N + Z$, can be written as [8]

$$E(Z, A) = f_B A + 4\pi R^2 \sigma + \frac{3Z^2 e^2}{5R} + E_{\text{pair}} + E_{\text{shell}}, \quad (1)$$

where f_B is the bulk energy contribution, which can be expressed as Taylor expansion [9] of u and x ($u = n/n_0$, $x = Z/A$). The radius of a nucleus is represented by R and σ is the surface tension. More precisely, we have

$$\begin{aligned} \sigma(x) &= \sigma_0 - (1 - 2x)^2 \sigma_\delta, \\ f_B(u, x) &= -B + S_v(1 - 2x)^2 + \frac{K}{18}(1 - u)^2, \\ E_{\text{pair}} &= -\frac{1}{2} [(-1)^N + (-1)^Z] \frac{\Delta}{\sqrt{A}}, \\ E_{\text{shell}} &= a_1 S_2 + a_2 S_2^2 + a_3 S_3 + a_{np} S_{np}. \end{aligned} \quad (2)$$

Table 1. Binding energy in MeV for selected nuclei.

| Nucleus | LDM | Expt. [10,11] |
|-------------------|-------|---------------|
| ^{16}O | 7.806 | 7.976 |
| ^{40}Ca | 8.625 | 8.551 |
| ^{48}Ca | 8.715 | 8.667 |
| ^{56}Fe | 8.780 | 8.790 |
| ^{62}Ni | 8.785 | 8.795 |
| ^{90}Zr | 8.697 | 8.710 |
| ^{132}Sn | 8.348 | 8.355 |
| ^{208}Pb | 7.878 | 7.867 |

We refer to Refs. [8,9] for details.

For the contribution from shell effects, we follow the prescription given by Duflo and Zuker [12], in which the shell energy contribution is written as a function of valence nucleons from the magic nuclei. Then S_2 , S_3 , and S_{np} are given by

$$\begin{aligned}
 S_2 &= \frac{n_v \bar{n}_v}{D_n} + \frac{p_v \bar{p}_v}{D_p}, \\
 S_3 &= \frac{n_v \bar{n}_v (n_v - \bar{n}_v)}{D_n} + \frac{p_v \bar{p}_v (p_v - \bar{p}_v)}{D_p}, \\
 S_{np} &= \frac{n_v \bar{n}_v p_v \bar{p}_v}{D_n D_p},
 \end{aligned} \tag{3}$$

where n_v (p_v) is neutron (proton) valence number, which is the minimum difference with the magic numbers: 2, 8, 20, 28, 50, 82, 126, and 184. For example, for the nucleus of $A = 50$, $Z = 23$, $N = 27$, $n_v = |27 - 28| = 1$, $p_v = |23 - 20| = 3$. D_n and D_p are the degeneracy of neutrons and protons, respectively, in the shell. Thus $D_{n=27} = 28 - 20 = 8$ in the above example. \bar{n}_v is the complementary valence number for neutron: $\bar{n}_v \equiv D_n - n_v$.

Using the measured masses of 2336 nuclei [10,11], we determine the parameter values (σ_0 , σ_δ , B , S_v , K , Δ , a_1, \dots, a_{np}) by minimizing the root-mean-square deviation. Table 1 shows a few examples for nuclear masses obtained by the LDM in the present work. Compared to other nuclear models such as Thomas-Fermi or Hartree-Fock calculations, LDM is fast for calculation and is quite successful to explain the experimental data. In addition, it can be further improved by adding other effects such as deformation effect, nuclear rotation, finite range surface term, and so on.

III. NEUTRON STAR CRUST

In the crust of neutron stars, nuclear matter is formed within the lattice structure. The BCC (Body-Centered-Cubic) is believed to be energetically the most favored form. In the outer core, nuclei are expected to exist with a free gas of electrons. As we go deeper into the crust of a neutron star, baryon number density increases and so does the mass number. Neutrons then drip out of heavy nuclei and start to form a free gas. As more and more free neutrons are accumulated, the inhomogeneity fades away and uniform nuclear matter is formed at the final stage. And, between the inner crust and outer core, nuclear pasta phase is expected to arise. The true ground state of nuclear matter highly depends on the shape. With increasing baryon number density, the distance between heavy nuclei decreases so that the nuclei undergo shape transitions. The first shape transition is into the cylindrical phase. The prolate nuclei are very close together and merged into a cylindrical shape. When the density increases more, the constituents of the cylindrical nuclear matter stick together to form a slab phase. Slab phase makes cylindrical holes (or bubble) as density increases, and cylindrical holes become bubble nuclei (spherical hole) and finally uniform nuclear matter is formed.

The numerical results of nuclear pasta phase can be found, for example, in Ref. 13. This pasta phase can be treated analytically in LDM. The energy density which is to be minimized using LDM is written as [14]

$$\begin{aligned}
 F &= u n_i f_i + \frac{3\sigma(x_i)s(u)}{r_N} + \frac{4\pi}{5}(r_N x_i e)^2 c(u) \\
 &\quad + (1-u) n_{no} f_o,
 \end{aligned} \tag{4}$$

where i (o) represents nuclear matter of dense (dilute) phase. Then f_i is the energy density of nuclei and f_o is that of free neutron gas in this case. Here, u is the volume fraction of nucleus to the Wigner-Seitz cell, while $s(u)$ and $c(u)$ are shape functions corresponding to the surface and Coulomb energy, respectively. The details can be found in Ref. 14. The total energy density of Eq. (4) is now minimized by varying u , n_i , x_i , n_{no} , and r_N with baryon number and charge neutrality conditions,

$$n = u n_i + (1-u) n_{no}, \quad n Y_p = u n_i x_i. \tag{5}$$

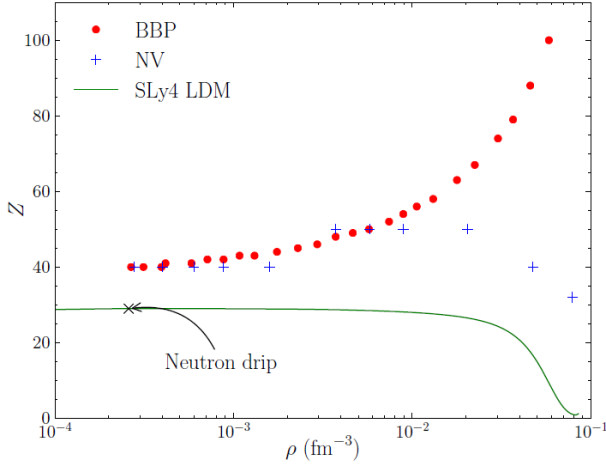


Fig. 2. (Color online) Atomic number of heavy nuclei in the crust of neutron stars.

The derivative of the energy density with respect to r_N gives the nuclear viral theorem which leads to $E_S = 2E_C$. This also allows the combination of shape functions, $s(u)$ and $c(u)$, to lead a smooth transition of each nuclear pasta phase [14] and we have

$$r_N = \left[\frac{15\sigma s(u)}{8\pi e^2 x_i^2 n_i^2 c(u)} \right]^{1/3} \equiv \frac{9\sigma}{2\beta} \left[\frac{s(u)}{c(u)} \right]^{1/3}, \quad (6)$$

$$E_S + E_C = \beta [s^2(u)c(u)]^{1/3} = \beta \mathcal{D}(u). \quad (7)$$

Nuclear pasta phase has discrete dimensions but the shape function $\mathcal{D}(u)$ allows continuous dimension for a given volume fraction u . This is justified because the energy difference among different pasta phase is small and quantum fluctuations between difference phases may happen.

Fig. 2 shows atomic number in the whole density range of a neutron star crust. Baym et al. [15] (BBP) utilized LDM to study the equation of state in the crust of neutron stars, while a more sophisticated calculation within Hartree-Fock (HF) approach was tried by Negele and Vautherin (NV) in Ref. 16. The differences in atomic number is caused by the numerical method used in numerical calculations. For example, BBP only deals with spherical nucleus in the Wiger-Seitz cell, while, within our approach, the nuclear pasta phase is considered systematically in the shape function $\mathcal{D}(u)$. The nuclei considered by NV also are restricted to spherical nuclei only. Because of HF properties, each nucleon wave function is to be calculated with proper boundary conditions.

IV. NEUTRON STAR CORE

In the core of neutron stars, all nuclei dissolve into uniform nuclear matter and the proton fraction is determined by giving the ground state energy. Mathematically, it can be written as

$$\mu_n = \mu_p + \mu_e, \quad \mu_e = \mu_\mu. \quad (8)$$

The above equation gives the proton fraction for a given baryon number density.

Since the density of the core in neutron stars can reach up to several nuclear saturation density, the chemical potential of neutrons and protons can exceed the rest mass of hyperons. Then the outcome of hyperons in the core results in a state whose energy is lower than the matter only with nucleons. For a unified description of neutron stars with hyperons, we first employ the relativistic mean field model (RMFM) to calculate nuclear EOS. In an RMFM, the nuclear force arises from the exchange of mesons such as σ , ω , and ρ mesons. We start with the effective Lagrangian for an RMFM which reads [8]

$$\begin{aligned} \mathcal{L} = & \bar{\Psi} \left[i \not{\partial} - g_\omega \psi - \frac{1}{2} \not{\phi} \cdot \vec{\tau} - M + g_\sigma \sigma - \frac{1}{2} e(1 + \tau_3) \not{A} \right] \Psi \\ & + \frac{1}{2} (\partial_\mu \sigma)^2 - V(\sigma) - \frac{1}{4} \Omega_{\mu\nu} \Omega^{\mu\nu} + \frac{1}{2} m_\omega^2 \omega^\mu \omega_\mu \\ & - \frac{1}{4} \vec{B}_{\mu\nu} \vec{B}^{\mu\nu} + \frac{1}{2} m_\rho^2 \vec{\rho}^\mu \cdot \vec{\rho}_\mu - \frac{1}{4} F_{\mu\nu} F^{\mu\nu} \\ & + \frac{\zeta}{24} g_\omega^4 (\omega^\mu \omega_\mu)^2 + \frac{\xi}{24} g_\rho^4 (\vec{\rho}^\mu \cdot \vec{\rho}_\mu)^2 \\ & + g_\rho^2 f(\sigma, \omega_\mu \omega^\mu) \vec{\rho}^\mu \cdot \vec{\rho}_\mu, \end{aligned} \quad (9)$$

where $\Omega_{\mu\nu}$ and $\vec{B}_{\mu\nu}$ are meson field strength tensors defined as $\Omega_{\mu\nu} = \partial_\mu \omega_\nu - \partial_\nu \omega_\mu$ and $\vec{B}_{\mu\nu} = \partial_\mu \vec{\rho}_\nu - \partial_\nu \vec{\rho}_\mu$, while $V(\sigma)$ is a scalar meson potential including the mass term:

$$V(\sigma) = \frac{1}{2} m_\sigma^2 \sigma^2 + \frac{\kappa}{6} (g_\sigma \sigma)^3 + \frac{\lambda}{24} (g_\sigma \sigma)^4. \quad (10)$$

The meson-meson interaction f -term is included to give a freedom to match asymmetric nuclear matter, which reads

$$f(\sigma, \omega_\mu \omega^\mu) = \sum_i^6 a_i \sigma^i + \sum_{j=1}^3 b_j (\omega_\mu \omega^\mu)^j. \quad (11)$$

Various relativistic models in the literature could explain the properties of finite nuclei quite successfully and we

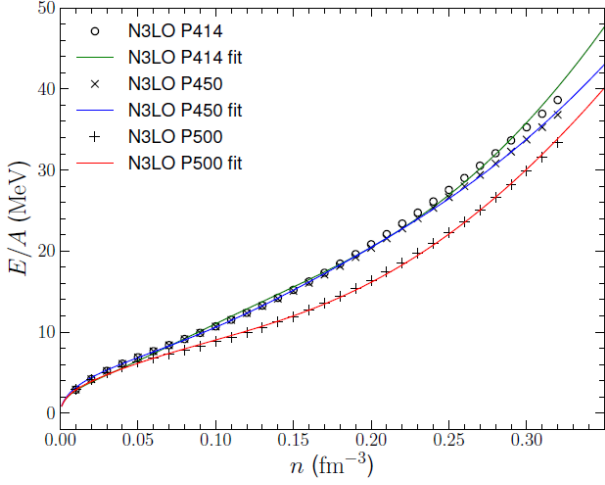


Fig. 3. (Color online) Energy per baryon from chiral effective field theory and from relativistic mean field model.

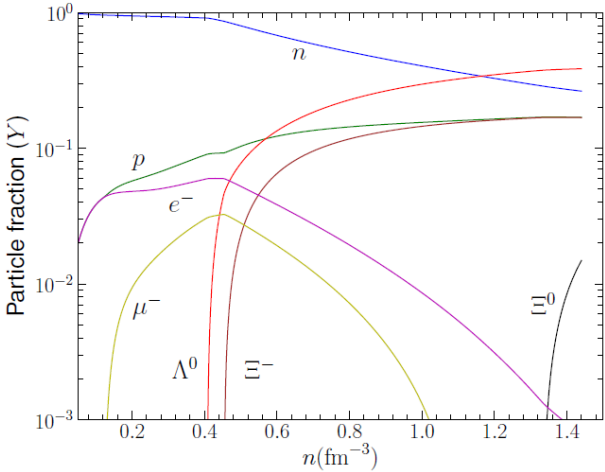


Fig. 4. (Color online) Particle fraction calculated from RMFM with the parameters fitted by P414 calculation and SU(6) meson-hyperon coupling constants.

can calculate density profiles, total binding energies, and spectrum of excited states, and so on. When we apply RMFMs to dense nuclear matter, however, we find that some of models cannot describe bulk nuclear matter correctly. This is because most of RMFM parameters were obtained by reproducing the properties of finite nuclei. Thus RMFMs are expected to be modified before being applied to neutron-rich nuclei. The neutron-rich nuclei, which normally have short lifetimes, are hard to synthesize but the construction of new facilities will shed light on our understanding of the structure and properties of such nuclei.

In this work, since we will use RMFM to investigate neutron star core, we first construct an RMFM whose

Table 2. Nuclear matter properties to fit the RMFM parameters. ζ is set to 0 to get the algebraic equations for symmetric nuclear matter. S_v and L are obtained after fitting the parameters. The normal nuclear density n_0 is in a unit of fm^{-3} , while the unit of B , K , S_v , and L is MeV.

| Model | n_0 | B | K | M^*/M_N | S_v | L |
|---------------|-------|------|-----|-----------|-------|-------|
| N3LO P414 fit | 0.16 | 16.0 | 235 | 0.75 | 31.64 | 47.78 |
| N3LO P450 fit | 0.16 | 16.0 | 235 | 0.75 | 31.43 | 47.37 |
| N3LO P500 fit | 0.16 | 16.0 | 235 | 0.75 | 28.06 | 33.07 |

parameters are fitted by pure neutron matter calculations. Recently, the pure neutron matter was studied using chiral effective field theory and quantum Monte Carlo simulations. In the present work, we adopt the N3LO (next-next-next leading order) chiral effective field theory (EFT) calculation of Ref. 17 to fit the RMFM parameters. Fig. 3 shows energy per baryon in neutron matter and the corresponding RMFM results. The notation in the model represents the cutoff momentum used in the EFT calculation. For example, P414 means that the cutoff momentum used in the calculation is $\Lambda_{cutoff} = 414$ MeV. Table 2 shows the nuclear matter properties calculated in this work. We set $\zeta = 0$ to get the algebraic equations for nuclear parameters related with symmetric nuclear matter properties such as n_0 , B , K , and M^* . The values of S_v and L are obtained from after the fitting procedure. Constructing an RMFM that explains both neutron matter and finite nuclei is very challenging and is beyond the scope of this work.

As explained before, the existence of hyperons in the core of neutron stars is expected as the chemical potential of the nucleon becomes larger than the effective mass of hyperons. The presence of hyperons in the core of neutron star can be considered within non-relativistic potential model or an extended RMFM. In RMFM, the introduction of hyperons can be done by extending the effective Lagrangian to include the hyperon interactions as

$$\mathcal{L}_{NN} \rightarrow \mathcal{L}_{NN} + \mathcal{L}_{YY}. \quad (12)$$

In the present work, we consider the SU(6) model for meson-hyperon interactions as described in Refs. [18,

19]. The relations between meson-hyperon and meson-nucleon coupling constant are given by

$$\begin{aligned} \frac{1}{3}g_{\omega N} &= \frac{1}{2}g_{\omega\Lambda} = \frac{1}{2}g_{\omega\Sigma} = g_{\omega\Xi}, \\ g_{\rho N} &= \frac{1}{2}g_{\rho\Sigma} = g_{\rho\Xi}, \quad g_{\rho\Lambda} = 0, \\ 2g_{\phi\Lambda} &= 2g_{\phi\Sigma} = g_{\phi\Xi} = -\frac{2\sqrt{2}}{3}g_{\omega N}. \end{aligned} \quad (13)$$

The σ - Y coupling constant are obtained from potential depth felt by hyperons in the bath of nucleons at the saturation as described in Ref. 20.

Fig. 4 shows the lepton and baryon fractions in the beta equilibrium nuclear matter. The Λ^0 is found to appear first because of its low mass, while leptons (e^- , μ^-) play a minor role as soon as Λ^0 and Ξ^- appear.

V. MASS AND RADIUS OF NEUTRON STARS

The macroscopic structure of neutron star can be obtained by solving general relativistic hydrostatic equation, which leads to the Tolman-Oppenheimer-Volkov equations:

$$\begin{aligned} \frac{dp}{dr} &= -\frac{G(M(r) + 4\pi r^3 p/c^2)(\epsilon + p)}{r(r - 2GM(r)/c^2)c^2}, \\ \frac{dM}{dr} &= 4\pi \frac{\epsilon}{c^2} r^2, \end{aligned} \quad (14)$$

where G is the Newton's gravitational constant and ϵ and p denote the energy density and pressure, respectively. The nuclear EOS provides energy density and pressure for a given baryon number density.

As can be seen in Fig. 5, the presence of hyperons in the core of neutron stars reduces the maximum mass of neutron stars. This is so-called ‘‘the hyperon puzzle’’ and there have been suggested many ideas to tackle this puzzle. This issue attracts recent research interests and new insights are called for to fully understand the role of hyperons in neutron stars.

VI. SUMMARY AND OUTLOOK

In the present work, we explained how to construct neutron star EOSs both in the crust and core of neutron

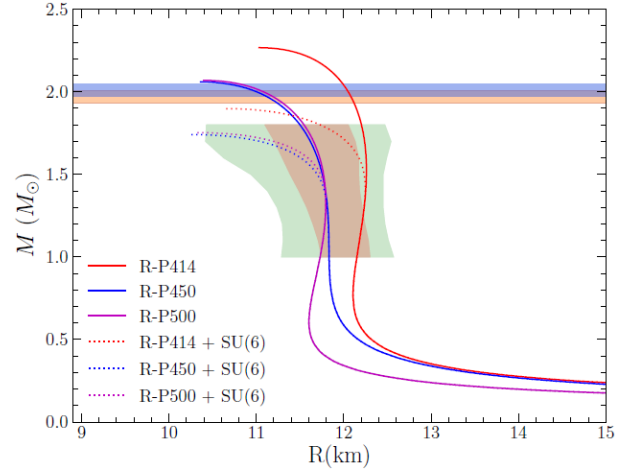


Fig. 5. (Color online) Mass and radius relation for several relativistic mean field models.

stars. We only consider zero temperature and ground state for nuclear matter. The generalization of neutron star EOS to finite temperature and arbitrary proton fraction will become supernovae EOS. The EOS for neutron star crust can be constructed using LDM, which is simple but powerful enough to explain binding energies of finite nuclei. The free gas of neutrons is consistently treated within the LDM formalism. The core of neutron stars consists of neutrons, protons, and electrons in the form of uniform matter. The derivative of total energy density with respect to proton fraction gives chemical equations. To understand the neutron star structure, we need more information on neutron-rich nuclei and the facilities under construction are expected to enlarge our knowledge for neutron-rich matter.

Despite the efforts to resolve the hyperon puzzle, the role of hyperons in neutron star is not fully understood. Widely used RMFM should be modified to include hyperon degrees of freedom and to explain the properties of finite nuclei and bulk properties of nuclear matter with isospin asymmetry. New ideas and approaches are, therefore, strongly called for to develop more realistic theory for neutron stars as well as precise new measurements on various properties of exotic nuclei in experiments.

ACKNOWLEDGMENTS

We are grateful to Ho-Meoyng Choi and Chang Ho Hyun for fruitful discussions. Y. Lim also thanks Jeremy

W. Holt for providing asymmetric nuclear matter EOS from chiral effective field theory calculations. The work of T.K. and Y.O. was supported by the National Research Foundation of Korea under Grant Nos. NRF-2015R1D1A1A01059603 and 2016K1A3A7A09005577.

REFERENCES

- [1] W. Baade and F. Zwicky, *Phys. Rev.* **46**, 76 (1934).
- [2] D. G. Yakovlev, P. Haensel, G. Baym and Ch. Pethick, *Usp. Fiz. Nauk* **183**, 307 (2013) [*Phys. Usp.* **56**, 289 (2013)].
- [3] A. Hewish, S. J. Bell, J. D. H. Pilkington, P. F. Scott and R. A. Collins, *Nature* **217**, 709 (1968).
- [4] P. B. Demorest, T. Pennucci, S. M. Ransom, M. S. E. Roberts and J. W. T. Hessels, *Nature* **467**, 1081 (2010).
- [5] J. Antoniadis, P. C. C. Freire, N. Wex, T. M. Tauris and R. S. Lynch *et al.*, *Science* **340**, 1233232 (2013).
- [6] A. W. Steiner, J. M. Lattimer and E. F. Brown, *Astrophys. J.* **722**, 33 (2010).
- [7] J. M. Lattimer and A. W. Steiner, *Astrophys. J.* **784**, 123 (2014).
- [8] A. W. Steiner, M. Prakash, J. M. Lattimer and P. J. Ellis, *Phys. Rep.* **411**, 325 (2005).
- [9] W. D. Myers and W. J. Swiatecki, *Ann. Phys. (N.Y.)* **55**, 395 (1969).
- [10] G. Audi, M. Wang, A. H. Wapstra, F. G. Kondev, M. MacCormick, X. Xu and B. Pfeiffer, *Chin. Phys. C* **36**, 1287 (2012).
- [11] M. Wang, G. Audi, A. H. Wapstra, F. G. Kondev, M. MacCormick, X. Xu and B. Pfeiffer, *Chin. Phys. C* **36**, 1603 (2012).
- [12] J. Duflo and A. P. Zuker, *Phys. Rev. C* **52**, R23 (1995).
- [13] M. Okamoto, T. Maruyama, K. Yabana and T. Tatum, *Phys. Rev. C* **88**, 025801 (2013).
- [14] J. M. Lattimer and F. D. Swesty, *Nucl. Phys. A* **535**, 331 (1991).
- [15] G. Baym, H. A. Bethe and C. J. Pethick, *Nucl. Phys. A* **175**, 225 (1971).
- [16] J. W. Negele and D. Vautherin, *Nucl. Phys. A* **207**, 298 (1973).
- [17] C. Wellenhofer, J. W. Holt and N. Kaiser, *Phys. Rev. C* **92**, 015801 (2015).
- [18] C. B. Dover and A. Gal, *Prog. Part. Nucl. Phys.* **12**, 171 (1985).
- [19] J. Schaffner, C. B. Dover, A. Gal, C. Greiner, D. J. Millener and H. Stöcker, *Ann. Phys. (N.Y.)* **235**, 35 (1994).
- [20] S. Weissenborn, D. Chatterjee and J. Schaffner-Bielich, *Nucl. Phys. A* **881**, 62 (2012).